Journal of Applied Fluid Mechanics, Vol. 16, No. 8, pp. 1666-1674, 2023.
Available online at www.jafmonline.net, ISSN 1735-3572, EISSN 1735-3645.
https://doi.org/10.47176/jafm.16.08.1680

Aerodynamic Investigation and Simulation Studies on Wing Section of an Unmanned Aerial Vehicle Attached with Solar Plate

D. Lakshmanan[1†], R. Boopathi[2] and P. Saravanan[3]

[1] *Department of Aeronautical Engineering, Bannari Amman Institute of Technology, Tamilnadu, 638401, India*
[2] *Department of Mechanical Engineering, Mahendra Engineering College, Tamilnadu, 637503, India*
[3] *Department of Aeronautical Engineering, Hindustan Institute of Technology and Science, Tamilnadu, 603103, India*

†*Corresponding Author Email: dlxaero@bitsathy.ac.in*

ABSTRACT

The paper investigates the aerodynamic performance and power requirement characteristics of wing sections integrated with high-lift airfoil to support the operation of solar-powered Unmanned Aerial vehicle (UAV). The flight mission is aimed to simulate the operation of solar-powered UAVs under low -speed environment. The research focuses on studying the aerodynamic effect of non-solar UAV wing model and solar UAV wing model for the varying angle of attack. The UAV wing models are tested using a subsonic wind tunnel to validate the aerodynamic characteristics at low-speed condition. The aerodynamic parameters such as coefficient of lift (C_l), coefficient of drag (C_d), coefficient of pressure (Cp), and the total power required to accelerate the solar UAV are studied to maintain steady level flight. The solar UAV and non-solar UAV wing models were subjected to a computational process to examine the pressure and velocity distributions for the aerodynamic performance analysis. Evident results show that the solar cells positioned at the flow separation region of the UAV wing model produces an aerodynamic efficiency rate of 5.45% and required 37.13W of minimum power compared to non-solar UAV at the Reynolds number of 9.8×10^6.

Article History

Received November 30, 2022
Revised April 2, 2023
Accepted April 10, 2023
Available online May 31, 2023

Keywords

Aerodynamics drag
Computational study
Solar cell
Unmanned Aerial Vehicle
Wind tunnel

1. INTRODUCTION

UAVs play a vital role in supporting the defence and military sectors for remote sensing and surveillance applications (Suraj et al., 2020). Expanding automobile industries have started to produce electric vehicles for commercial purposes to occupy complete space in modern society (Halil et al., 2015). According to the survey of energy utilization, the transition from traditional fuels to renewable sources is improved in all aspects of commercial utilization over decades. The readily available and renewable solar energy could be effectively utilized for making UAVs for longer flight hours. The flight endurance of traditional UAVs is severely affected owing to their insufficient propulsive energy generation process (Mamdouh, 2003). It is essential to provide longer flight hours for UAVs operated to achieve advanced missions including border surveillance, reconnaissance, aerial surveying, and emergency medical services. Ashleigh et al. (2020). studied the variety of energy sources utilized for operating unmanned aerial vehicles. Hence, chemical propulsive products were integrated to accelerate the UAVs and long-lasting flight endurance was achieved through the natural source of energy. Kyosic and Hoyon (2018). modeled the solar-powered UAV with 160 kg of mass subjected to the different phases of the flight profile. Their investigation recommended that the maximum rate of climb was achieved at the lowest possible minimum safety speed during the flight test. Besides, it increased the operating speed and affected the rate of energy consumption predominantly by impacting the endurance of solar UAVs. Alan et al. (2019) revealed the process of increasing the endurance capabilities with batteries charging process through the solar cells mounted on the UAV and performed the gliding flight. Parvathy and Howard (2018) proposed a conceptual methodology and compared the power consumption rate of high-endurance solar UAVs and Non-solar UAVs. The sufficient thrust was generated for the solar UAV model and it was greater than 25% of the take-off mass that supported faster acceleration and quick climbing to higher altitudes at flight test. The hybrid airfoil FX-60 was utilized by Ziheng et al. (2021). for miniature solar UAV wing mounted with a conventional Li-Po battery for power generation. The results show that the improper sizing of solar cells aerodynamically impacts the issues on the flight mission as the model is subjected

Nomenclature

A_f	frontal area of the UAV	P	power required
C_d	coefficient of drag	S	span
C_l	coefficient of lift	T	thrust
C_p	coefficient of pressure	V	air velocity (UAV speed in real condition)
c	chord	W	weight
D	drag force	τ	shear stress
L	lift force	ρ	density of air
p	surface pressure	θ	inclination angle of port in degree
p_∞	static pressure	α	angle of attack

to basic maneuverings. The electric energy supplied to the propulsive system of a UAV could be effectively balanced through the utilization of solar cells. Moreover, the weight reduction on UAVs enhanced the generation of lifting force and improves flight hours. Rowayne et al. (2020). numerically found the lift component of a conventional solar UAV increased to 9% per meter at low Reynolds number 2×10^5 for the constant speed. The airfoil E-216 was modified to the span of 73m with more cells on the optimized wing structure Panayiotou et al. (2016). potentially attained the required solar energy during the flight test and notified fewer vortices around the surface area. Findings show that unpiloted flight vehicles must be operated at low speed and in lower altitude environment to maintain the sufficient aerodynamic efficiency. Spedding and McArthur (2010). examined the efficiency of wing structure conditionally subjected to computational simulation for low speed at the Reynolds number10^5. Though meteorological conditions determine the irradiation level of solar energy, the possibility of extending the flight duration is achieved only through the integration of solar cells into the UAV structure. Yauhei et al. (2021). Conducted an open flight test and compared the endurance capabilities of conventional radio-controlled RC planes and solar cell UAVs. Their investigation was evident that the durability and flight hours of a modified solar cell UAV increased by 25% over the conventional RC plane. However, earlier research on UAVs notably addressed the issues related to the performance parameters such as flight endurance, power consumption rate, and aerodynamic ineffectiveness to maintain continuous flight. Though few relevant studies have shown the impact of operational parameters on the performance of UAVs, none of the researchers explored the combined effect of aerodynamic parameters and power requirements of solar UAVs operated at low-speed environments for the past decades. It is essential to study the aerodynamic efficiency of optimized solar-powered UAVs configured for long-endurance flight missions. Hence, this research is carried out to study the aerodynamic coefficients and power requirements of UAV wing models attached to solar cells. An optimized wing section designed with a high-lift airfoil positioned with solar cells at the flow separation point of the solar UAV wing model was investigated numerically and experimentally in the low-speed environment to enhance aerodynamic efficiency.

2. MISSION AND METHOD

In military aviation operations, UAVs were frequently utilized at hazardous distant places for achieving complicated long endurance missions. Owing to their limitation in endurance, the solar-powered UAVs fly slowly and capture the incident radiations of sunlight during the phases of the flight mission (Panagiotou et al., 2016). To capture higher solar power, the operating speed of solar UAVs is mapped to the solar irradiation by receiving the capacity of solar cells during the flight test (Alan et al., 2019). Aimed to produce more electric power and long endurance, the wing structure of solar-powered UAVs is optimized with the number of solar cells on the upper surface (Chih-Wei et al., 2010). In this research, the flight mission specifications of solar-powered UAVs are presented in Table.1.

The wing section is configured to the span (*b*) of 6m and sized to 1.2 m chord length (*c*) whereas, the wing surface area is calculated as 7.2 m^2. Figure 1. Shows the eight solar cells that are mounted over the starboard and port side of the wing surface area to accelerate the 2kg of UAV wing model. Though the UAV model has integrated the solar cells on the entire wing, considering any one side of the wing satisfied the accuracy of results observed in the experimental and numerical simulation process (Xinhua et al., 2020).

Table 1 Mission specifications.

Parameters	Unit (S.I)
Mass of the plane	2 (kg)
Payload	0.25 (kg)
Atmospheric air density	1.225 kg/m^3
Wing Span	6 (m)
Airfoil	Eppler 387
Operating velocity	25 m/s

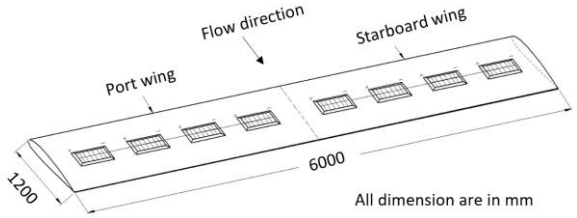

Fig. 1. Schematic of solar-powered UAV wing.

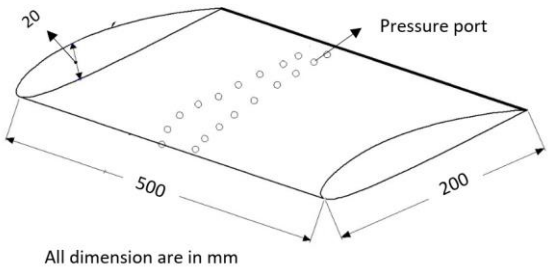

Fig. 2. UAV wing model with pressure port arrangements.

The highly reliable solar cell sun-power-C60 contains sectional dimensions of 70mm×70mm and is utilized for capturing the irradiation energy.

3. EXPERIMENTAL SETUP

The experimental studies are carried out with a subsonic speed open circuit wind tunnel which is equipped at Bannari Amman Institute of Technology, Erode, India. The variable speed subsonic wind tunnel contains a test section area of 600mm × 600mm and is capable of operating at 50 m/s. The test section is provisioned with Pitot static tube to measure the velocity component at the top whereas, the sixteen-channel pressure scanner is connected to the side wall portion and is directly mounted to the UAV wing model. The wind tunnel test is moreover performed preferably with wing models scaled down from the actual dimensions that are quite interesting in the integration process. To attain real-time results, kinematics and geometric similarities between the actual and scaled model are to be studied with Reynold`s law. However, the main objective of the present study focuses to understand the flow physics and the aerodynamic effect of solar cells mounted on the UAV wing model. Hence, the geometric similarity is properly ensured for the UAV wing model used in this present study. Since the necessity of achieving absolute accuracy is not essential and is witnessed from the comparative analysis, (Nelson et al., 2016). The experimental results observed in this present study for the solar UAV wing model and the non-solar UAV wing model are compared and validated with the literature data. The geometric similarity is achieved at a 1:6 length scale ratio was uniformly maintained based on the existing Solvendus UAV model. The optimized UAV wing model (span 500 mm, chord 200 mm, and thickness 20 mm) is shown in Fig. 2. Experimental model was developed through PLA 0.75mm filament material subjected to 3-D printing process and coated with laminated sticker for surface finishing. The pressure ports were embedded on the surface of the fabricated UAV wing model aligned to the center line and ensured the proper flow of streamlined patterns. Hence, the upper and lower surfaces of the model impinged with 12 pressure ports on each side and a port at the leading edge of the airfoil for stagnation pressure measurement were depicted in Fig. 2. The port numbers P1 to P12 are placed at the upper surface whereas the P13 to P24 is fixed at the lower surface. The P0 is considered

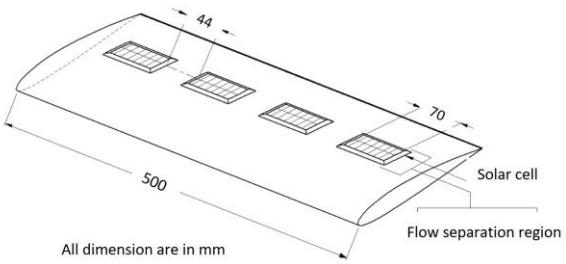

Fig. 3. Schematic of solar cells arrangements and dimensions.

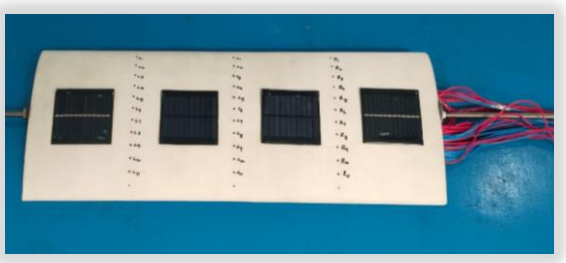

Fig. 4. Solar cells and pressure arrangements on UAV wing model.

a stagnation port impinged near the leading edge of the UAV wing model (Sivaraj et al., 2018).

Figures 3 & 4. Show the arrangement of solar cells in a series of patterns and polished with coating materials to avoid surface roughness. The UAV model is integrated with four solar cells and equally spaced with 44mm. The same model is utilized for the preliminary experimental process is shown in Fig. 5.

The surface pressure measurements are carried out for the non-solar UAV wing model and solar UAV wing model with constant flow conditions over the operating velocity of 25 m/s and Reynolds number of around 9.8×10^6. Based on the experimental surface pressure measurements, the aerodynamic performance parameters such as the coefficient of pressure (Cp), coefficient of drag (C_d), and coefficient of lift (C_l) are obtained using Eq.(1), Eq.(2) & Eq.(3) for the non-solar and solar UAV wing models.

$$C_p = (P - P_\infty) / 0.5\,\rho U^2 \quad (1)$$

$$C_d = \int_0^\pi (Cp \times \cos\theta \times l)/h \quad (2)$$

$$C_l = \int_0^\pi (Cp \times \sin\theta \times l)/h \quad (3)$$

Fig. 5. Open circuit subsonic wind tunnel with UAV wing model.

Where C_d – Coefficient of drag; C_p – Coefficient of pressure, *l*- length of the pressure port on the wing surface from front end in m, *h* -height of the pressure port on the wing surface from the bottom in m, *P*-surface pressure, P_∞ - static pressure, *U* – velocity of air inside the test section, θ – inclination angle of port in degree and C_l – coefficient of lift.

At a steady level Thrust (T) = Drag (D) and Lift (L) = Weight (W), the thrust required to maintain the solar UAV is revealed in Eq. (4) (Daniel, 2012).

$$T = D = \frac{1}{2}\rho v^2{}_\infty A_f C_D \quad (4)$$

Moreover, the solar UAV is required to throttle with minimum power to maintain a steady level (Karthik and Aneesh 2017). The power required to accelerate the solar UAV in terms of drag components and operating velocity is examined in Eq. (5).

$$P = [Total\ drag\ (D) \times V_{Cruise}]\ W \quad (5)$$

The solar UAV equipped with a motor assembly and battery unit generates the required Total power (*P*) to maintain the accelerative flight.

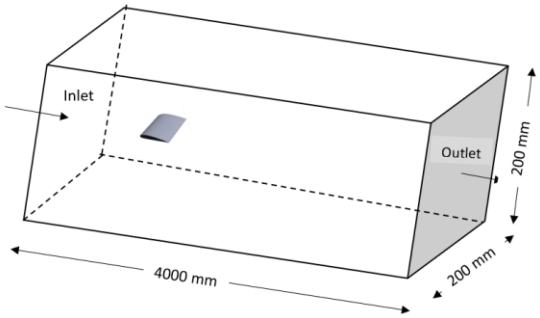

Fig. 6. Computational domain with dimensions.

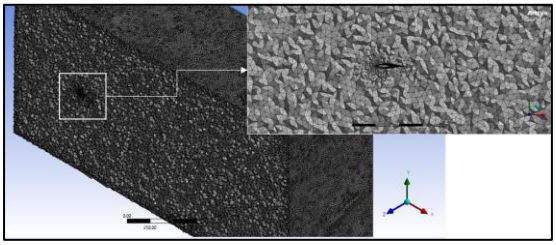

Fig. 7. Unstructured mesh on UAV wing model.

4. NUMERICAL STUDY

Taking into account the limitations and requirements of validation in the experimental results, numerical simulation is performed to observe the aerodynamic behavior around the non-solar and solar UAV wing model using ANSYS-Fluent 18.0 for the constant flow conditions. The geometry construction of the UAV wing model with and without solar cells is sized to a 1:6 scale ratio and utilized for the experimental study and the same is subjected to the numerical analysis using a solid works package (Morgado et al., 2016). The computational domain sized to the cuboid structure contains 4000 mm (length)×2000 mm (height) and 2000 mm (width) projected in Fig. 6. Dimensions of the computational domain around the UAV wing model in length, height and width were indicated as 20c, 10c, and 10c respectively. The surface elements of the computational domain framed with an inlet, outlet, top, and bottom were projected in Fig. 6

The Delaunay triangulation method is used to construct the unstructured meshes with tetrahedral element shown in Fig. 7. The mesh size was calculated based on the global element size of the cells with the necessary parameters that govern the size of the UAV model surface mesh. All the parameters of the prism layer contain a growth rate of 1.2 and a y+ value tuned to 30. The flexibility in y+ values is provided at the range of 30-300 to maintain the smooth conduct of the simulation process. A good-quality grid is attained with an aspect ratio of less than 3 for 90% of its element. The fine-unstructured mesh applied to the surface of the UAV wing model and computational domain edges is subjected to coarsely unstructured mesh. The grid independence study is carried out for the simulated UAV wing model with four different mesh elements. Meshes sized to mesh 1-321542, Mesh 2-384217, Mesh 3- 442921, and Mesh 4-491163. The course mesh is converted to fine mesh elements for accuracy enhancements. At the initial stage, flow over a UAV wing model without solar cell was imported to the numerical simulation of the K-∈ model with ANSYS Fluent 18.0 for a constant velocity of 25 m/s at the Reynolds number of 9.8×10^6 (Bharath et al., 2017). The grid independence study predicts the reduction in computational time at Mesh 3 with 442921 cells whereas the convergence attained an accurate level. The Coarse and Fine meshes can differ by 32% which is adequate for mesh independence analysis. The boundary conditions of the UAV wing model at the inlet opted for a steady flow velocity of 25 m/s and the outlet pressure is maintained the same as the operating pressure.

The pressure-based solver integrated with k-ϵ turbulence model and is utilized for investigating the computational performance parameters of the UAV wing model (Jin et al., 2014). The continuity Eq. (6) and momentum Eq. (7), Eq. (8) & Eq. (9) equations of the structured domain are solved with finite volume computational fluid dynamics code for the imported UAV wing model.

Continuity equation $\frac{\partial \rho}{\partial t} + \nabla.(\rho.V) = 0 \quad (6)$

X-momentum equation

$$\frac{\rho\partial(u)}{\partial t} + \nabla.(\rho.u.V) = -\frac{\partial P}{\partial x} + \frac{\partial \tau_{xx}}{\partial x} + \frac{\partial \tau_{yx}}{\partial y} + \frac{\partial \tau_{zx}}{\partial z} + \rho f_x \quad (7)$$

Y-momentum equation

$$\frac{\rho\partial(v)}{\partial t} + \nabla.(\rho.v.V) = -\frac{\partial P}{\partial y} + \frac{\partial \tau_{xy}}{\partial x} + \frac{\partial \tau_{yy}}{\partial y} + \frac{\partial \tau_{zy}}{\partial z} + \rho f_y \quad (8)$$

Z-momentum equation

$$\frac{\rho\partial(w)}{\partial t} + \nabla.(\rho.w.V) = -\frac{\partial P}{\partial z} + \frac{\partial \tau_{xz}}{\partial x} + \frac{\partial \tau_{yz}}{\partial y} + \frac{\partial \tau_{zz}}{\partial z} + \rho f_z \quad (9)$$

The numerical simulation for the solar UAV and non-solar UAV wing model incorporated governing equations which attained the convergence in 10^{-6} order. During the post-processing, the interaction of flow fields over the

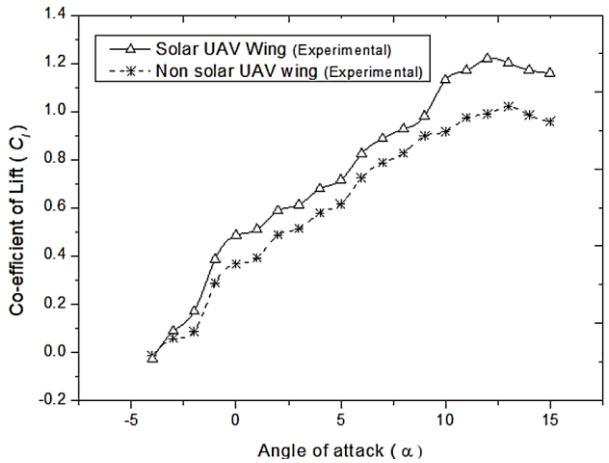

Fig. 8. Coefficient of lift C_l trends for the angle of attack α.

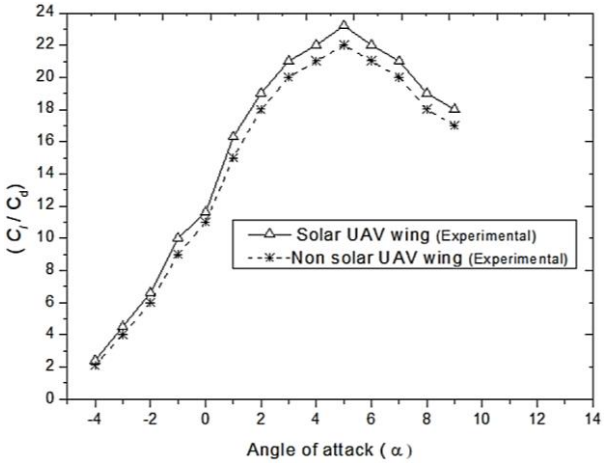

Fig. 9. Aerodynamic coefficients C_l/C_d trends for the angle of attack α.

UAV wing model is visualized to the multiple cross sections in the 3-D environment. The aerodynamic coefficients and velocity profiles are obtained for solar and non-solar UAV wing models to study the flow behavior in the low-speed environment.

5. RESULTS AND DISCUSSION

To analyze the aerodynamic performance of non-solar and solar UAV wing models the experimental work found the variation of aerodynamic coefficients such as

coefficient of lift (C_l), coefficient of drag (C_d), coefficient of pressure (C_p), and aerodynamic efficiency C_l/C_d for the varying angle of attack to analyze the aerodynamic performance of non-solar and solar UAV wing models. The surface pressure measurement data from the wind tunnel test is utilized to examine the coefficient of pressure (C_p) at Eq. (1) whereas, the coefficient of drag (C_d) and coefficient of lift (C_l) is analyzed with Eq.(2) & Eq.(3). The drag coefficients (C_d) are subjected to Eq. (4) and obtained the thrust required to maintain the steady level flight. The numerical simulation process showed the distribution of the pressure field and velocity field over the wing surface area of non-solar and solar UAV models to examine the flow behaviors at low Reynolds number regions.

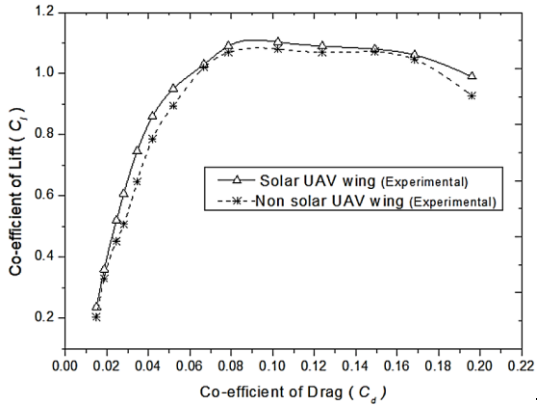

Fig. 10. Comparison of C_l and C_d with α for solar and non-solar UAV wing model.

5.1 Aerodynamic Analysis - Experimental Method

Figure 8. found that the solar and non-solar UAV wing models produced sufficient upward forces and reached the maximum value of the coefficient of lift C_l before reaching the stalling point. Further, the lift coefficient C_l increased with an increase in angle attack for the solar UAV wing model and attained a negligible amount of stalling region compared to non-solar UAV. At $\alpha = 12°$, the coefficient of lift C_l reached 1.21 for the solar UAV whereas, the non-solar UAV attained the C_l of 0.98 for the same angle of attack. The high-lift airfoil integrated with solar and non-solar UAV wing sections produced positive lift even at a negative angle of attack owing to their high-cambered leading edges (John 2010).

The drag polar graph (From Fig. 9) predicts the aerodynamic efficiency of non-solar and solar UAV wing models for the varying angle of attack. At $\alpha = 5°$ the aerodynamic efficiency has reached 22.22% for the non-solar UAV wing model whereas, the solar UAV wing model has reached 23.43% for the same angle of attack. Hence, the rate of aerodynamic efficiency increased by 5.45% for the solar UAV compared to non-solar UAV. Figure 10. shows the distribution of the coefficient of lift C_l and coefficient of drag C_d for the varying angle of attack. The non-solar UAV wing model generates continuous increments in the coefficient of lift C_l and drag coefficient C_d for the angle of attack ranges - 4° to 6°. Moreover, the solar UAV wing model produces maximum values of coefficient of lift C_l and drag coefficient C_d for the angle of attack ranges -4° to 6° compared to non-solar UAV. And for the angle of attack 6° to 12°, the coefficient of lift C_l attained the maximum value whereas, the rate of increment in drag coefficient C_d becomes very less compared to non-solar UAV.

The distribution of coefficient pressure over the upper and lower surfaces of solar and non-solar UAV wing models is presented in Fig. 11. It is noted that the flow separation at the upper surface of a non-solar UAV wing experiences the maximum negative pressure near the trailing edge and wake regions compared to the solar UAV wing model. At $\alpha=10°$ angle of attack, the non-solar UAV wing model produces remarkable flow separations at $0.4c$ chord length. To delay the flow separation of non-solar UAV wing model for the same angle of attack, the solar cells are attached at the flow separation region. The

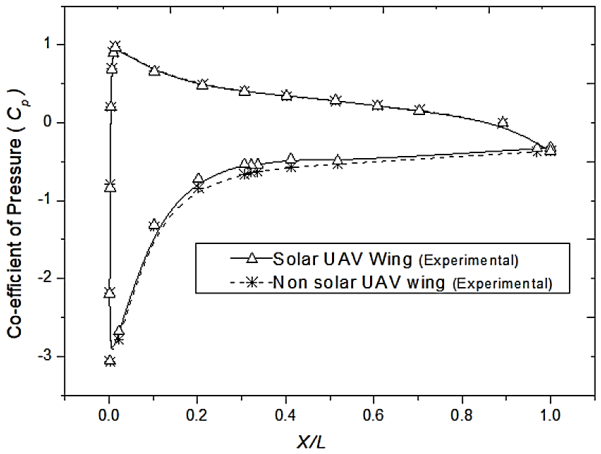

Fig. 11. C_p distribution of solar and non-solar UAV wing model.

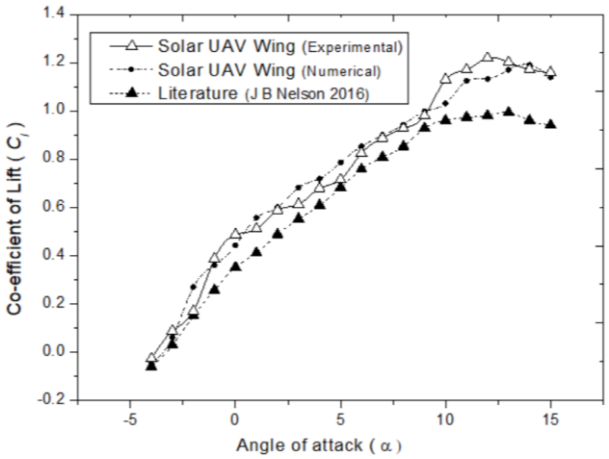

Fig. 12. Comparison of C_l with α for Experimental, Numerical, and Literature.

experimental results show that the flow separation delayed to *0.9c* chord length for the solar UAV wing model. Hence, findings show smooth flow patterns and reduced negative pressure region at the upper surface area compared to the non-solar UAV wing model.

Existing works of literature show that an Unmanned Aerial Vehicle flying at low altitude for more than 25 m/s produces the flow separation phenomenon over the wing section and thereby causes energy loss in the flow. Further, it indirectly increases the negative pressure and produces a drag force over the wing. Hence, solar cells are placed at the flow separation region on the wing surface of the UAV. The flow over the protrusion surfaces of the solar cells produces reattachment in the flow patterns and re-energizes the flow. Hence, it delays the formation of flow separation and is attached to the flow over the wing surface. The physics of flow is shown evidently in Fig. 11 which indicates the variation of coefficient of pressure (*Cp*) distribution over the UAV wing models.

5.2 Aerodynamic Analysis - Numerical Method

Further the numerical simulation is performed to understand the closeness of experimental results observed for the solar and non-solar UAV wing models. Though numerical simulation is an approximate solution, it is essential to validate the numerical results with existing research and experimental data. Accordingly, the comparative results (Fig. 12) obtained from the numerical simulation, experimental and existing literature are presented for the solar UAV wing model trends for the coefficient of lift (C_l) versus varying angle of attack (α). The coefficient of lift (C_l) increases with increases in the angle of attack (α) and it is observed that the numerical results are in-line with the experimental and existing literature research, (Nelson et al., 2016).

The numerical computational process shows the pressure and velocity distribution contours of non-solar UAV (a) and solar UAV (b) wing models integrated with high-lift airfoil for the constant velocity of 25m/s. Figure 13 and Fig. 14 Shows the maximum pressure distribution at the stagnation point near the leading edges of the non-solar and solar UAV wing model. Hence upper and lower surfaces of the UAV wing model contribute sufficient pressure contours for generating the required lifting force.

The non-solar UAV wing model experienced the flow separation region at the 2/3rd of chord length and observed the trailing edge vortices for the same velocity (Guo et al. 2013). Solar cells attached at the flow separation region over the upper surface of the solar UAV wing model brought the flow reattached and witnessed the continuous smooth flow patterns. Hence, the low-pressure region is reduced to 3/4th of the chord length and the solar UAV wing model produces high pressure at the rear side over the upper surface area owing to the reduction in the flow separation process.

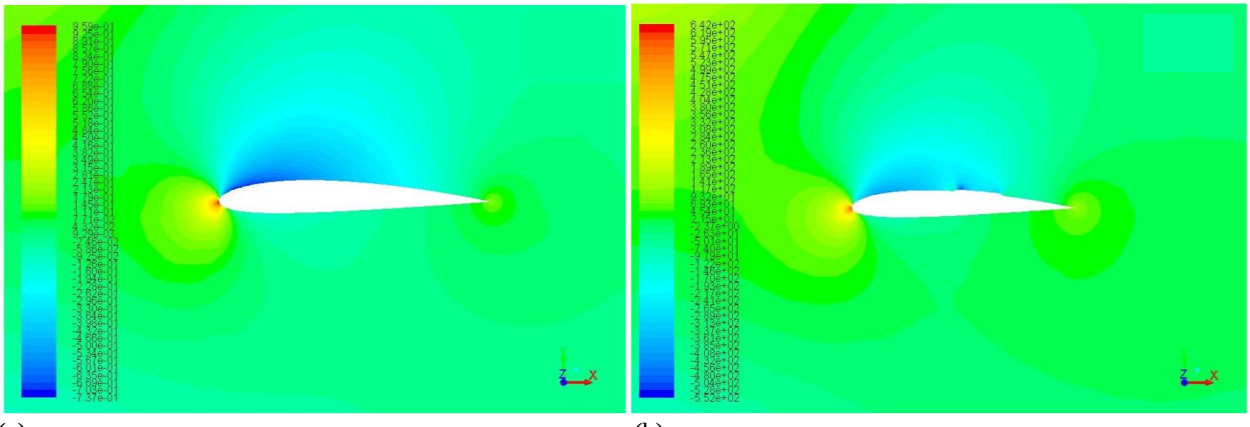

(a) (b)

Fig. 13. Pressure distribution at mid plane of UAV wing model (a). Non-solar UAV & (b). Solar UAV.

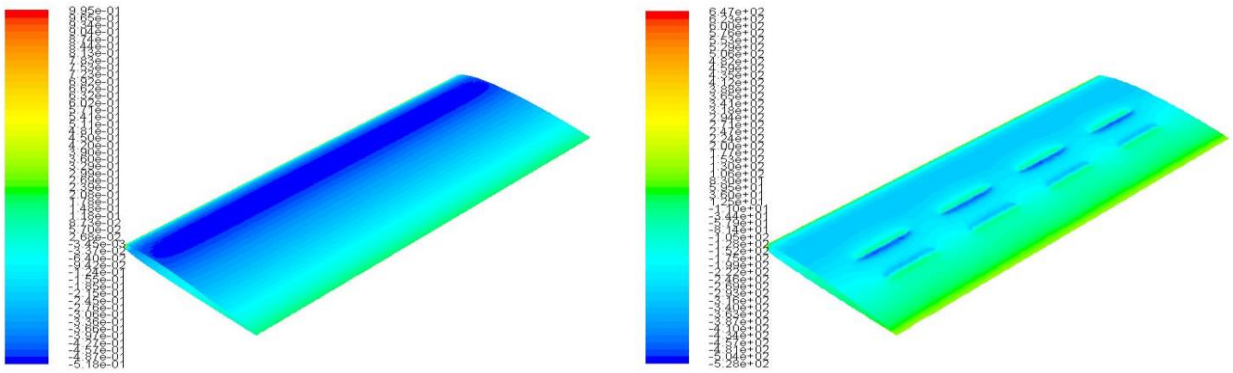

(a) (b)

Fig. 14. Pressure distribution over UAV wing model (a). Non-solar UAV & (b). Solar UAV.

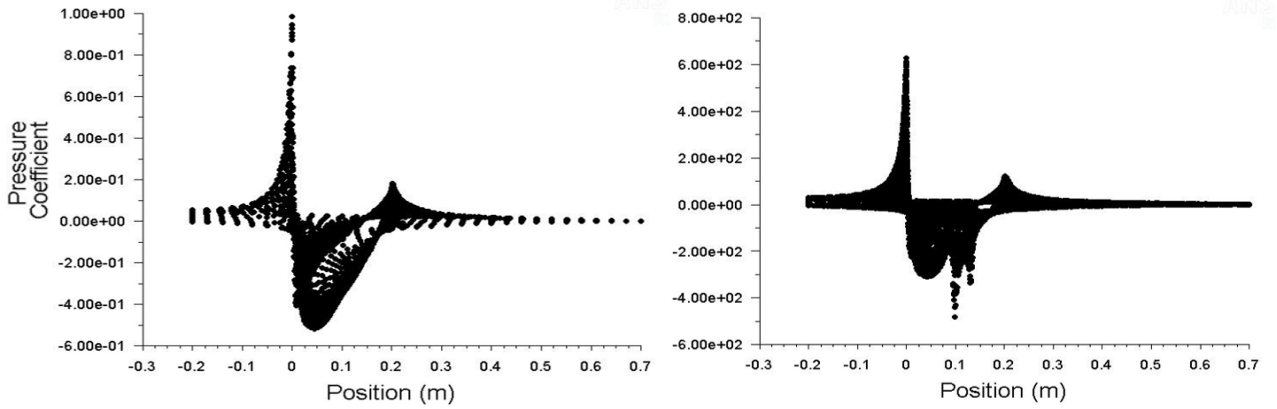

(a) (b)

Fig. 15. C_p trends for position of UAV wing model (a). Non-solar UAV & (b). Solar UAV.

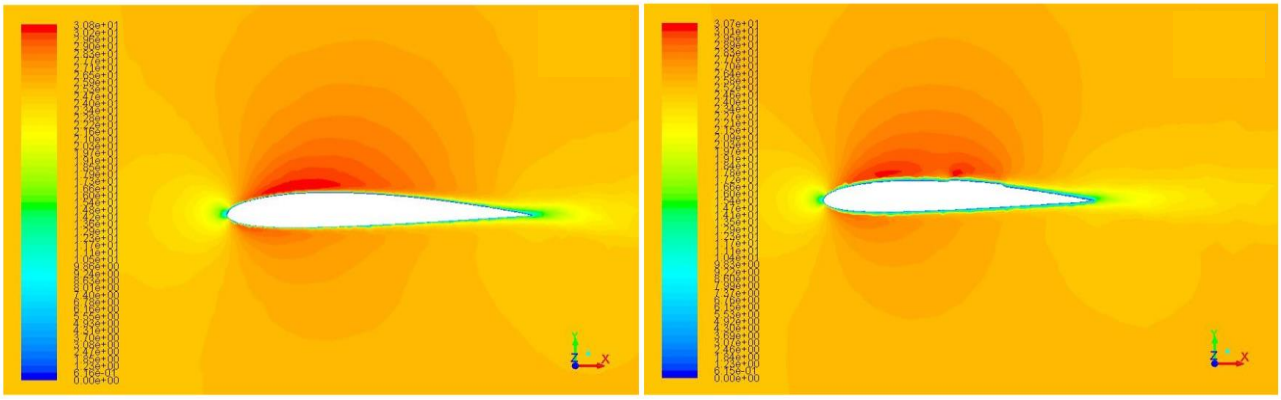

(a) (b)

Fig. 16. Velocity distributions at mid plane of UAV wing model (a). Non-solar UAV & (b). Solar UAV.

Table 2 Thrust and Power.

Angle of Attack (Degree)	Total Power (W)
α=2°	7.00
α=9°	19.64
α=13°	37.13

Figure 15. indicates that the low-pressure region has predominantly increased over the upper surface area along the position (0.3-0.7) for the non-solar UAV wing model. The high-pressure regions are formed for the position length ranges 0.2-0.7 for the non-solar UAV wing model. Figure 16. reveals the velocity distributions of detached and reattached flow patterns of non-solar and solar UAV wing models for the constant velocity of 25m/s. The decelerated flow patterns observed at the *0.6c* chord length for non-solar UAV and continuous attached flow patterns found to the chord length of *0.9c* for the solar UAV wing model.

Further the research has found the thrust force and power required to operate the solar UAV model which is presented in Table 2.

The requirement of thrust and power components of the solar UAV wing model increased with the increase in the angle of attack. Hence, the solar UAV model throttled to supply sufficient power respective to altitude gain. The operating velocity of solar UAV decreases respectively

with changes in the angle of attack, (John 2010). Karthik and Aneesh (2017). examined the airfoil we-3.55 series-based conventional wing solar-powered UAV. It requires 40.11W of total power to lift 2 kg of take-off mass at the constant operating speed. Hence the research revealed, the high-lift airfoil-based solar UAV model requires a minimum power of 37.13W to maintain a steady level at constant operating speed for the same gross weight. Results witnessed the effect of positioning the solar cells ahead of the flow separation point on the UAV wing model which increased the rate of aerodynamic efficiency to 5.45% contributing to form smooth flow behaviour and required a minimum power of 37.4W to operate the 2kg of solar powered UAV at a steady level.

6. CONCLUSION

The research study was conducted to analyse the aerodynamic effect of solar cells attached to UAV wing models. The preliminary UAV wing models were investigated experimentally and numerically for varying angles of attack. The aerodynamic coefficients of solar and non-solar UAV wing models were examined to enhance the aerodynamic efficiency. The minimum power required to operate the designed solar UAV model at the low-speed environment was studied for the varying angle of attack. Results recommend that mounting the solar plates at the flow separation over the solar UAV wing model has attained the maximum aerodynamic efficiency of 23.43% and delayed the flow separation phenomenon at the upper surface. To conclude, the research also found that the aerodynamically balanced UAV wing models controlled the power requirements needed to maintain steady and level flight.

ACKNOWLEDGEMENTS

The authors would like to thank the Department of Aeronautical Engineering for their support during the wind tunnel testing at Bannari Amman Institute of Technology for continuous guidance and expertise.

CONFLICT OF INTEREST

The authors have no conflict of interest to disclose in this research work.

AUTHORS CONTRIBUTION

D. Lakshmanan: Developed conceptualization, methodology, and validation.

R. Boopathi: Performed writing - Oral draft preparation.

P. Saravanan: Performed writing - reviewing and editing.

REFERENCES

Alan, G. E., Reyes, O., Luis, A. B., Omar, L. B., Octavio, G. S., & Patricia, Z. R. (2019). Conceptual design of an unmanned fixed-wing aerial vehicle based on alternative energy. *International Journal of Aerospace Engineering*, 1(1), 1-10. https://doi.org/10.1155/2019/8104927

Ashleigh, T., Immanuel, N. J., Christiaan, M., Dmitri, B., & Rupert, G. (2020). A comprehensive review of energy sources for unmanned aerial vehicles, their shortfalls and opportunities for improvements. *Heliyon*, 6(11), 1-9. https://doi.org/10.1016/j.heliyon.2020.e05285

Bharath, G., Hikaru, O., Inderjit, C., & Justin, W. (2017). Basic understanding of airfoil characteristics at low reynolds numbers. *Journal of Aircraft*, 55(1),1-23. https://doi.org/10.2514/1.C034415

Chih, W. C., Der, M. M., Jaw, K. S., & Jie, R. S. (2010). Optimal sizing and cruise speed determination for solar powered airplane. *Journal of Aircraft*, 47(2), 622-629. https://doi.org/10.2514/1.45908

Daniel, P. (2012). *Aircraft Design - A conceptual Approach*. sixth edition, American Institute of Aeronautics and Astranautics incorporated, Virginia.

Guo, F., Huang, C. & Lei, J. (2013). Numerical study of separation on the trailing edge of a symmetrical airfoil at a low Reynolds number. *Chinese Journal of Aeronautics*, 26(4), 918-925. https://doi.org/10.1016/j.cja.2013.06.005

Halil, C,. Kadir, A. D., & Nafiz, A. (2015). Unmanned aerial vehicle domain: Areas of research. *Defence Science Journal*, 65(4), 319-329. https://doi.org/10.14429/dsj.65.8631

Jin, W., & Lee, Y. G. (2014). Computational analysis of the aerodynamic performance of a long endurance UAV. *International Journal of Aeronautical and Space sciences*, 15(4), 374-382. https://doi.org/10.5139/IJASS.2014.15.4.374

John, D. A. (2010). *Fundamentals of Aerodynamics*. fifth edition, McGraw-Hill Education Publishing Ltd, United States.

Karthik, R. B. S., & Aneesh, P. (2017). Performance analysis of solar powered unmanned aerial vehicle. *Renewable Energy*, 104(1), 20-29. https://doi.org/10.1016/j.renene.2016.12.008

Kyosic, S., Jon, A., & Hoyon, H. (2018). Mission analysis of solar UAV for high-altitude long-endurance flight. *Journal of Aerospace Engineering*, 31(3), 1-10. http://dx.doi.org/10.1061/(ASCE)AS.1943-5525.0000832

Mamdouh, G. S. (2003). Can renewable and unconventional energy sources bridge the global energy gap in the 21st Century. *Applied Energy*, 75(1),33–42. https://doi.org/10.1016/S0306-2619(03)00016-3

Morgado, J., Pascoa, J. C., Silvestre, M .A. R., & Vizinho, R. (2016). XFOIL vs.CFD performance predictions for high lift low reynolds number airfoils. *Aerospace Science and Technology*, 52(1), 207-214. https://doi.org/10.1016/j.ast.2016.02.031

Nelson, J. P. B., Julio, E. P. V., John, J. V. R., Pedro, D. B., & Hernan, D. C. (2016).Design and manufacture

of a solar powered unmanned aerial vehicle for civilian surveillance Missions. *Journal of Aerospace Technology and Management*, 8(4), 385–396. http://dx.doi.org/10.5028/jatm.v8i4.678

Panagiotou, P., Tsavlidis, I & Yakinthos, K. (2016). Conceptual design of a hybrid solar MALE UAV. *Aerospace Science and Technology*, 53(1), 207-219. https://doi.org/10.1016/j.ast.2016.03.023

Parvathy, R., & Howard, S. (2018). Development of design methodology for a Small solar-powered unmanned aerial vehicle. *International Journal of Aerospace Engineering*, 2018, 1-10. https://doi.org/10.1155/2018/2820717

Rowayne, E. M., Mehdi, N., & Amanda, J. H. (2020). Solar powered unmanned aerial vehicle: A numerical approach in improving solar cell performance. *International Journal of Aerodynamics*, 7(1),61-82. https://doi.org/10.1504/IJAD.2020.107162

Sivaraj, G., Paramasivam, K., & Suganya, G. (2018). Reduction of aerodynamic drag force for reducing fuel consumption in road vehicle using basebleed, *Journal of Applied fluid mechanics*, 11(6),1489-1495. http://dx.doi.org/10.1088/1742-6596/1888/1/012016

Spedding, G. R., & McArthur, J. (2010). Span Efficiencies of Wings at Low Reynolds Numbers. *Journal of Aircraft*, 47(1), 120-128. http://dx.doi.org/10.2514/1.44247

Suraj, G., Shivam, S., & Ankur, D. (2020). Review of solar unmanned aerial vehicles(UAV) and its sustainability. *Engineering Technology and Research*, 2(1),001-006. https://doi.org/10.15413/etr.2020.108

Xinhua, L., Kaijun, S., & Feng, L. (2020). General optimal design of solar powered unmanned aerial vehicle for priority considering propulsion system. *Chinese Journal of Aeronautics*, 33(8), 2176-2188. https://doi.org/10.1016/j.cja.2020.04.009

Yauhei, C., Chunleung, H., Yoonjo, L., & Boyang, L. (2021) Development of a solar powered unmanned aerial vehicle for extended flight endurance. *Drones*, 5(2),1-19. https://doi.org/10.3390/drones5020044

Ziheng, L. (2021). *Prototype of a solar powered fix-winged unmanned aerial vehile*. IOP Conference series: *Journal of Physics* 1(1),1-9. https://doi.org/10.1088/1742-6596/2029/1/012016